Rheotaxis-based separation of sperm with progressive motility using a microfluidic corral system

Meisam Zaferani[a], Soon Hon Cheong[b], and Alireza Abbaspourrad[a,1]

[a]Department of Food Science, College of Agriculture and Life Sciences, Cornell University, Ithaca, NY 14853; and [b]Department of Clinical Sciences, College of Veterinary Medicine, Cornell University, Ithaca, NY 14853

Edited by Howard A. Stone, Princeton University, Princeton, NJ, and approved July 3, 2018 (received for review January 15, 2018)

The separation of motile sperm from semen samples is sought after for medical infertility treatments. In this work, we demonstrate a high-throughput microfluidic device that can passively isolate motile sperm within corrals inside a fluid channel, separating them from the rest of the diluted sample. Using finite element method simulations and proposing a model for sperm motion, we investigated how flow rate can provide a rheotaxis zone in front of the corral for sperm to move upstream/downstream depending on their motility. Using three different flow rates that provided shear rates above the minimum value within the rheotaxis zone, we experimentally tested the device with human and bovine semen. By taking advantage of the rheotactic behavior of sperm, this microfluidic device is able to corral motile sperm with progressive velocities in the range of 48–93 $\mu m \cdot s^{-1}$ and 51–82 $\mu m \cdot s^{-1}$ for bovine and human samples, respectively. More importantly, we demonstrate that the separated fractions of both human and bovine samples feature 100% normal progressive motility. Furthermore, by extracting the sperm swimming distribution within the rheotaxis zone and sperm velocity distribution inside the corral, we show that the minimum velocity of the corralled sperm can be adjusted by changing the flow rate; that is, we are able to control the motility of the separated sample. This microfluidic device is simple to use, is robust, and has a high throughput compared with traditional methods of motile sperm separation, fulfilling the needs for sperm sample preparation for medical treatments, clinical applications, and fundamental studies.

sperm separation | medical infertility treatment | microfluidic | rheotaxis

Sperm motility is required for sperm to traverse the female genital tract, reach the site of fertilization, and penetrate the cumulus extracellular matrix around the oocyte and zona pellucida (1, 2). According to clinical reports, 10% of couples worldwide are infertile (3, 4), and almost half of these infertility cases are due to male infertility as a result of low sperm motility (2). Assisted reproductive technologies (ARTs), such as intrauterine insemination, in vitro fertilization, and intracytoplasmic sperm injection, are used clinically to overcome infertility. All of these infertility treatments include an initial step of separating motile sperm with acceptable morphology from the semen sample. There is some evidence that improvement in the quality of collected sperm can increase the likelihood of successful insemination (5, 6).

Two methods currently exist for the separation of sperm with desirable motility characteristics, including swim-up and density gradient centrifugation. However, these techniques are time- and labor-intensive. Furthermore, they are not wholly selective, isolating abnormal as well as desirable motile sperm (3, 6, 7). The sperm swim-up method requires the semen sample to be centrifuged (200–400 × g), which is hazardous to sperm morphology and has a relatively low yield (8). Density gradient centrifugation exposes semen samples to even greater centrifugal force as well as free radical-mediated DNA damage, which may threaten paternal content and be hazardous to the morphology of the sperm cell (4, 9, 10).

The development of methods to isolate motile sperm, especially methods that circumvent centrifugation, would benefit infertility treatments and improve our understanding of sperm biology. The factors that influence the journey of a sperm cell, which starts with ejaculation and ends with egg fertilization, are poorly characterized. Some efforts have investigated the response of sperm to external stimuli, like chemical gradients and fluid flow; such responses are generally referred to as "taxis" (10, 11). Researchers have also investigated the tail-beating patterns of sperm in different situations (12–14), as well as the molecular interactions between sperm and the female reproductive tract (1, 14–16). However, since the study of sperm in vivo is complicated by the existence of many environmental variables, such as pH, chemical gradients, and fluid flow (2, 10, 11), many questions about sperm behavior remain unanswered. The concurrent existence of these variables impedes our ability to gain better insight into sperm motion itself, which is a complex topic (17). Thus, the isolation of motile sperm in vitro (eliminating all external hydrodynamic velocity fields and dead sperm) could further assist the study of sperm locomotion. Additionally, isolating sperm in a particular region would enable the evaluation of an individual sperm's biological and physiological responses to a specific chemical or physical factor (18). To summarize, any improvement toward separation and/or isolation of motile sperm from the rest of the semen sample would be an achievement in facilitating the study of mammalian reproduction.

Microfluidic systems are promising tools of fluid manipulation, which could be used to successfully separate and analyze sperm (19). With exquisite precision at small scales (2 μm–1 mm), microfluidics can enable us to manipulate microswimmers (i.e., microorganisms that swim using a flagella) more easily compared with traditional methods and with fewer drawbacks, as no centrifugal force is

Significance

The separation of motile sperm from semen samples is required for medical infertility treatments and clinical studies. Conventional methods are time- and labor-intensive and could be potentially hazardous to morphology and paternal content of the sperm. Using a microfluidic corral system and the ability of viable sperm to swim against flow, we were able to passively isolate motile sperm from the semen sample inside a corral. This device can separate sperm with velocities higher than a cutoff, which is tunable with the injection rate. The unprecedented efficiency of our device in comparison to previous studies and its benign passive nature make it favorable for sperm separation.

Author contributions: M.Z. and A.A. designed research; M.Z. performed research; M.Z., S.H.C., and A.A. contributed new reagents/analytic tools; M.Z. analyzed data; M.Z., S.H.C., and A.A. wrote the paper; S.H.C. provided intellectual input about biological aspects of the research; and A.A. was principal investigator of the group intellectual inputs.

The authors declare no conflict of interest.

This article is a PNAS Direct Submission.

[1]To whom correspondence should be addressed. Email: alireza@cornell.edu.

This article contains supporting information online at www.pnas.org/lookup/suppl/doi:10.1073/pnas.1800819115/-/DCSupplemental.

Published online July 30, 2018.

required. Additional advantages include low sample consumption and the capability of automation. Recently developed microfluidic technology has been applied to investigate the physical aspects of sperm locomotion and chemotaxis. One such device guides sperm in a counterclockwise direction in a "one-way street" to investigate the effects of structural changes of the microfluidic device on sperm movement (17). Other studies have investigated the inclination of sperm to swim near rigid boundaries (20–24), and another experimental study has provided a theoretical model for the rheotactic behavior of sperm (25) [i.e., their proclivity to swim in the opposite direction of the surrounding fluid flow (26)].

In the past decade, some microfluidic devices have been proposed for ART applications (27–29), including those that have been used to separate sperm (30). In one effort, a passive microfluidic system called microscale integrated sperm sorter (MISS) was proposed that could separate motile sperm from the rest of the sample (8). Although the motility of the separated sample using this device was reported as ∼100%, the presence of sperm with nonprogressive and abnormal motility in the separated fraction lowers the effectiveness of this technique. Additionally, the device provides no tunability to modify the motility distribution of the separated sperm, demonstrating the technique's low precision. Active microfluidic methods have also been reported (18, 31, 32), in which external active forces, such as hydrostatic pressure, optical traps, and magnetophoresis, are used for sperm separation. However, these techniques are not suitable for the isolation of healthy sperm (8), being too invasive. In addition, complex experimental setups are required for these active methods, making them time- and labor-intensive.

In this study, we present a microfluidic device that can noninvasively and passively separate motile sperm from the rest of the semen sample in a precise and tunable manner. This design relies on the rheotactic behavior of sperm. Employing this device, we demonstrate the isolation of motile human and bovine sperm in a corral-shaped feature inside the microfluidic channel. To generate a rheotaxis zone in front of the corral, where only sperm with normal and progressive motility are able to swim upstream, and thus enter the structure, we performed finite element method (FEM) simulations to determine appropriate injection rates of the sperm medium. Moreover, we experimentally measured a minimum shear rate within the rheotaxis zone required for sperm to reorient upstream. We subsequently demonstrated that this separation method provides enhanced precision in sperm selection by experimentally extracting the sperm movement distribution within the rheotaxis zone, measuring the velocity distribution of the captured sperm, and proposing a theoretical model for sperm motion within this zone. This separation method is highly tunable in regard to the motility of the isolated sample, providing marked improvement in comparison to established sperm isolation methods. No dead sperm or sperm with abnormal motility were observed within the corral; thus, 100% of the separated sperm exhibit normal and progressive motility, which is an unprecedented advantage of this separation technique. Finally, by designing and incorporating sperm retainers inside the corral, we made our device more stable, increasing the residence time of the sperm from ∼12 s to more than 45 min.

Results and Discussion

Mechanism of Sperm Separation and Simulations. The ability of sperm to swim upstream (33) enables these microswimmers to travel distances over 10,000-fold longer than their head-to-tail length to fertilize an oocyte. This important attribute of sperm results from the hydrodynamic interactions of sperm with walls and the front/back asymmetry of their shape (21). In the absence of an external fluid flow, sperm locomotion is roughly circular in both right- and left-handed modes (11). However, in the presence of an external fluid flow, different torques exist on the head and tail of the sperm due to the difference in resistive forces applied to each. This generates a rotation, causing sperm to orient themselves in the opposite direction of the fluid influx. This mechanism is utilized by sperm as a navigational system to track and fertilize the oocytes (34). The upstream swimming, rheotactic behavior of sperm is observed for a discrete shear rate of the surrounding fluid (11, 24, 33). A minimum threshold shear rate for sperm orientation is required, while shear rates above the maximum threshold will prevail over the force produced by the sperm flagellum (25). There are some reports suggesting that velocities in the range of 27–110 $\mu m \cdot s^{-1}$ for bovine sperm and 22–102 $\mu m \cdot s^{-1}$ for human sperm can lead to sperm rheotaxis (11, 21, 24). For this reason, we decided to begin our microfluidic investigations at these two velocity ranges, as they are consistent with the typical physical and biological properties experienced by the sperm samples.

Unlike the forces produced by the medium flow, sperm progressive motility that results from the flagellum's propulsive force (2) cannot contribute to its upstream orientation. Once a sperm swims in a shear flow, its head will be closer to the top surface of the corral system, where it is barely influenced by the flow, while its tail experiences a greater force, as shown in Fig. 1*A*. Based on the resistive force theory, the torque resulting from this situation rotates the sperm in the top view plane around its pivot (head) as depicted in Fig. 1*B*. The angular velocity of this rotation (Ω) can be described by Eq. **1** (21):

$$\Omega = \frac{d\theta}{dt} = -A\gamma \sin\theta, \qquad [1]$$

in which γ is the shear rate of the sperm medium near the wall (viable sperm mostly swim in the vicinity of the wall) and A is a constant related to the geometry of the microswimmer (21, 35). This rotation is temporary, and once the sperm finds its consistent orientation ($\theta = 0$), it starts swimming upstream with the propulsive force provided by the flagellum (22).

On the basis of this rheotactic behavior of sperm, we propose a microfluidic channel design featuring seven interior corrals. The width of the channel, its depth, and the outer and inner radii of the corrals are 500 μm, 30 μm, 150 μm, and 100 μm, respectively (Fig. 1*C*). The rationale behind this design is to create rheotaxis zones in front of each corral using appropriate sperm medium injection rates, thus enabling motile sperm that pass through these regions to reorient themselves and begin swimming toward the opposite direction of the flow until they enter the interior of the corral structure and become trapped. In this manner, healthy and motile sperm can be separated from the rest of the sample, which includes dead, abnormal (motility lower than the minimum cutoff), and misproportioned microswimmers (in which abnormal morphology affects motility).

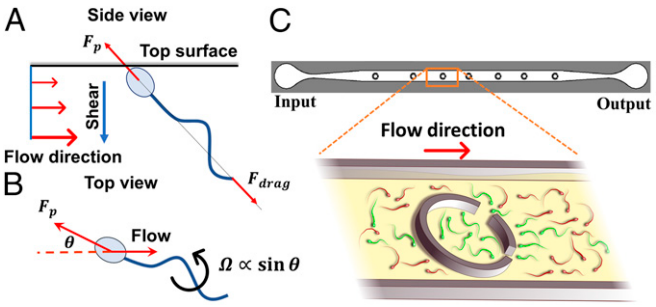

Fig. 1. Minimal hydrodynamic model for the upstream orientation of sperm. (*A*) Side view of the sperm in the vicinity of the top surface. The sperm tail experiences a greater force than its head. F_p, sperm propulsive force. (*B*) Top view of sperm. The rotation caused by shear leads to an upstream orientation. F_{drag}, the drag force imposed by the surrounding fluid. (*C*) Polydimethylsiloxane-based microfluidic device featuring seven corrals inside the channel.

The velocity field of the sperm medium in the rheotaxis zone should be gentle enough for viable sperm to swim upstream (11) compared with the surrounding velocity in the channel, in which they cannot overcome the flow. Since the corral is an obstacle in the middle of the microfluidic channel, the velocity field of the sperm medium in front of it will be lower than above or below this feature. Thus, using the corral as a barrier, we can create an area in front of this structure in which the velocity field is gentler than in any other region throughout the channel. As illustrated in Fig. 1*C*, dead sperm (shown in red) move along the fluid streamlines, but normal and viable sperm (shown in green) can swim upstream in front of the corral and eventually enter it, becoming trapped. While some of the motile and live sperm do not enter the rheotaxis zone, and consequently cannot enter the corral, all of the sperm that do enter this zone, and are motile enough to swim upstream, will enter the corral.

To produce a gentle flow in front of the corrals that encourages the upstream swimming behavior of motile sperm (thus trapping them inside the structures), we conducted FEM simulations to estimate an appropriate range for the sperm medium injection flow rate. Momentum and mass conservation equations were solved using no-slip boundary conditions at the walls, enabling us to extract the velocity field across the microfluidic layout. The velocity field within the channel is expressed in colors, as can be seen in Fig. 2 *A*–*C*, so that red represents the maximum velocity (~480 $\mu m \cdot s^{-1}$) and blue corresponds to zero velocity. The velocity field is expressed in Y–Z cut planes at four different positions, as can be seen in Fig. 2*A*, and the contour levels corresponding to each of these positions are demonstrated in Fig. 2*B*. We also demonstrated the velocity field in an X–Y cut plane featuring a depth half as large as the depth of the channel in Fig. 2*C*, in which the direction of the velocity field at each calculated point is depicted using arrows. Within the corral, the velocity field is zero and the medium is shown to be quiescent. Since transportation of dead sperm relies on drag force, the absence of streamlines entering the corral supports our previous assertion that no dead sperm can enter the structure.

The rheotactic behavior of the sperm in the vicinity of the microfluidic channel's top surface is correlated to the shear rate of the fluid in that region in the Z direction. Therefore, we calculated the shear rate distribution on the top surface, which is shown in Fig. 2*D* for an injection rate of 1.2 $mL \cdot h^{-1}$. In this figure, the yellow color corresponds to a shear rate of $\gamma = 8.21\ s^{-1}$, while the minimum shear rate ($\gamma = 0$) is shown in black. Since the evolution of sperm orientation is determined by the shear rate in proximity to the top surface, this shear profile throughout the structure and in the vicinity of its top surface was required to simulate sperm movement in front of the corral. Moreover, to experimentally determine the minimum shear rate required for sperm to undergo rheotaxis, the shear rate in the rheotaxis zone must be known.

To provide a more vivid understanding of the fluid flow in front of the corral, we reported the velocity field for different flow rates (0.6–1.8 $mL \cdot h^{-1}$ with steps of 0.12 $mL \cdot h^{-1}$) along the X axis, where X is shown in Fig. 2*D*. According to the simulations, the velocity field of the sperm medium is zero near the corral wall. As X increases, the velocity field of the medium also increases, until it finally reaches a constant value ranging from 110–135 $\mu m \cdot s^{-1}$ (depending on the injection rate) at ~300 μm from the corral (Fig. 2*E*).

If the shear rate in the rheotaxis zone is above a threshold value, then all of the motile sperm will be able to orient themselves in an upstream direction, with the angular velocity varying depending on the shear rate at the reorientation point. However, reorientation cannot guarantee the entrance of sperm into the corral. Sperm must be motile enough to overcome the fluid flow. Therefore, the fraction of the sperm that are motile enough to move toward the corral depends on the velocity field within the rheotaxis zone. Higher flow rates lead to a smaller fraction,

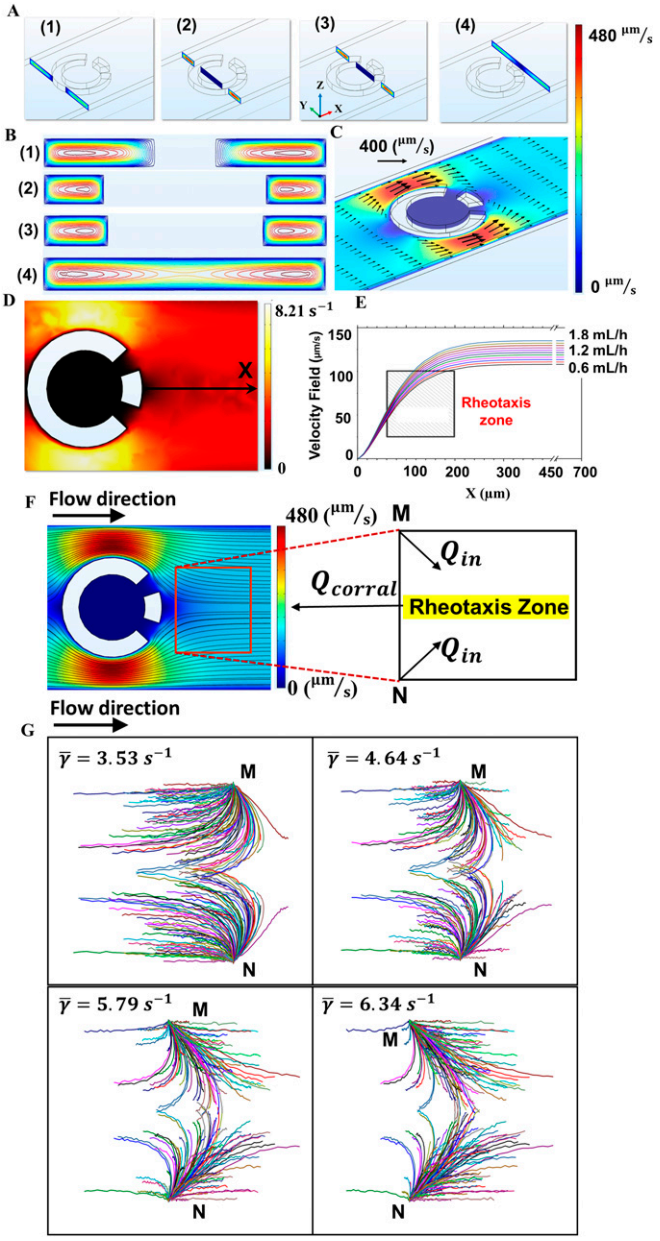

Fig. 2. Simulation-based velocity field of the sperm medium and trajectories extracted for sperm inside the rheotaxis zone. (*A*) Velocity field of the semen sample medium is calculated and presented in four different Y–Z cut planes. Red correlates to the maximum value of the velocity field (480 $\mu m \cdot s^{-1}$), whereas blue corresponds to zero. (*B*) Velocity fields of the Y–Z cut planes are drawn in contour levels. (*C*) Velocity field around the corral at an injection rate of 1.2 $mL \cdot h^{-1}$ in an X–Y cut plane. (*D*) Shear rate in the vicinity of the top surface. (*E*) Velocity field of the sperm medium along the X axis. (*F*) Rheotaxis zone in front of the corral is depicted, and the medium velocity field and shear rate in the zone are calculated by FEM simulations. This zone is a hypothetical area in front of the corral in which sperm entering it are likely to enter the corral. The sperm enter the rheotaxis zone from points M and N with Q_{in} (the number of sperm entering the rheotaxis zone per second). A portion of these sperm will enter the corral at the rate of Q_{corral} (the number of sperm entering the corral per second). (*G*) Equations of sperm motion were solved for 400 sperm with velocities between 40 $\mu m \cdot s^{-1}$ and 90 $\mu m \cdot s^{-1}$ following a normal distribution with a mean value of 65 $\mu m \cdot s^{-1}$. As the flow/shear rate increases, the number of sperm moving upstream toward the corral (Q_{corral}) drops. $\bar{\gamma}$ is the mean value of the shear rate within the rheotaxis zone.

whereas lower flow rates increase the portion; therefore, the resolution of the motility-based sperm selection in the corral is proportional to the velocity field within the rheotaxis zone.

To model and calculate the fraction of sperm that can enter the corral as a function of flow rate, we solved the equations of the sperm motion within the rheotaxis zone (Fig. 2*F*). We assumed that sperm propulsive velocity does not change over time and its direction evolves as Eq. **1** describes. We also assumed that sperm have a lateral head movement that can be modeled as white Gaussian noise, $\xi(t)$, using $\langle \xi(t)\xi(t') \rangle = \delta(t-t')$. We solved the equations of the motion for 400 sperm with a normal velocity distribution and a uniform initial direction, entering the rheotaxis zone from the top left (point M) and the bottom left (point N) corners with the rate of Q_{in} (i.e., the number of sperm entering the rheotaxis zone per second) (Fig. 2*F*). As the flow/shear rate increases, the number of sperm moving upstream decreases, as can be seen in Fig. 2*G*. Consequently, it was expected that the shape of the sperm velocity distribution inside the corral would be narrower as the flow rate increases.

Experimental Results of Motile Sperm Separation. In addition to simulations, we studied the motion of sperm in the fabricated microfluidic device featuring seven corral structures. The dynamic of trapped sperm inside an individual corral for both bovine and human samples is shown at different times in *SI Appendix*, Fig. S1. According to these images (also Movies S1 and S2), the trapped sperm are motile and viable, and their motilities are seemingly normal (~65–89 $\mu m \cdot s^{-1}$ for bovine and 58–81 $\mu m \cdot s^{-1}$ for human samples). All of the isolated sperm have a regular tail-beating pattern and normal lateral head movement, and they all show a strong tendency to swim in proximity to the interior walls of the corral (also Fig. 3 and the trajectories of the sperm). In *SI Appendix*, Fig. S1*A*, at t = 1 s, a bovine sperm enters the corral, and at t = 10 s, the number of isolated bovine sperm has increased to 10 (*SI Appendix*, Fig. S1*B*). In addition to the increasing number of isolated sperm, the dynamic of sperm inside the corral includes their hydrodynamic interactions with the interior walls. In fact, once the sperm encounter the interior walls, they start rotating to swim along the walls, and, most of the sperm eventually accumulate near the interior wall, as can be seen in *SI Appendix*, Fig. S1*B*. An increase in the number of isolated sperm and accumulation near the interior wall are also observed for human sperm (*SI Appendix*, Fig. S1 *C* and *D*). Since the velocity field inside the corral is negligible, this observation is not correlated to the velocity field of the sperm medium outside the corral.

To validate our hypothesis that rheotactic behavior can guide sperm toward the corrals, we made video recordings of sperm movement inside the microfluidic device. As shown in Fig. 3 *A* and *B*, bovine and human sperm, respectively, were tracked swimming upstream and entering the corral. In Fig. 3 *A* and *B*, the red ovals label sperm that are undergoing rheotaxis, whereas the yellow ovals indicate sperm that have already been isolated within the corral and have stopped moving upstream, returning to their original flow-free swimming pattern. These figures highlight only a small portion of the total number of sperm (~150) swimming upstream to convey the separation mechanism.

We extracted the trajectories of both bovine and human sperm and demonstrate them in Fig. 3 *C* and *D*, respectively, in which black circles represent the starting point of each trajectory. Based on these patterns, we can see that the sperm begin to swim upstream once they enter the rheotaxis zone behind the corral. It takes less than 2 s for the sperm to transition their swimming direction toward the opposite direction of the flow. Based on the earlier theoretical model provided, this orientation of the sperm cell is anticipated, and we already know that the time of the rotation is correlated to the shear rate around the sperm close to the wall. This change of direction is discernible in the trajectories of some sperm in both Fig. 3 *C* and *D*, as indicated with arrows; as illustrated, most of these trajectories finish near the interior wall of the corral.

In addition, to quantitatively assess the role of rheotaxis in increasing the isolation efficiency of motile sperm inside the corral device, and to experimentally confirm the theoretical model, we investigated the distribution of movement of the sperm in front of the corral as a function of flow rate The distribution of the movement status of the sperm for both human and bovine samples is presented in *SI Appendix*, Figs. S2–S4, which demonstrated that the percentage of upstream-reoriented sperm within the rheotaxis zone was ~35–50%. This percentage shows us that providing the rheotaxis zone in front of the corral increased the number of isolated sperm. Our experimental results agreed with the corresponding corral tunability in capturing the sperm, as predicted by simulation-based results; the values acquired from the experimental data are juxtaposed with the simulation-based results for both human and bovine sperm samples and are demonstrated in *SI Appendix*, Fig. S5. Eventually, to determine the minimum shear rate at which sperm can undergo rheotaxis and reorient themselves upstream, we experimentally extracted the swimming distribution for sperm within the rheotaxis zone for three different flow rates, including 0.1 $mL \cdot h^{-1}$, 0.5 $mL \cdot h^{-1}$, and 0.6 $mL \cdot h^{-1}$ (*SI Appendix*, Fig. S6), and we found that the minimum shear rate required for sperm to display rheotactic behavior was $\gamma_{min} = 3.43 \pm 0.12\ s^{-1}$.

To quantitatively report the motility of the captured sperm, we calculated the velocity distribution of the isolated microswimmers inside the corral (*SI Appendix*, Fig. S7). To calculate the velocity of a single sperm, we measured the progressive distance covered by the motile sperm. Next, by dividing this distance by the elapsed time, we were able to obtain the average progressive velocity of each sperm. These velocities were measured inside the corral, where the velocity field is zero. As a result, the reported velocity of the sperm is solely due to their own propulsion force. We observe that the velocity of sperm with maximum abundancy (in terms of the number of isolated sperm) is not associated with the input flow rate (*SI Appendix*, Fig. S7). As long as the injection flow rate

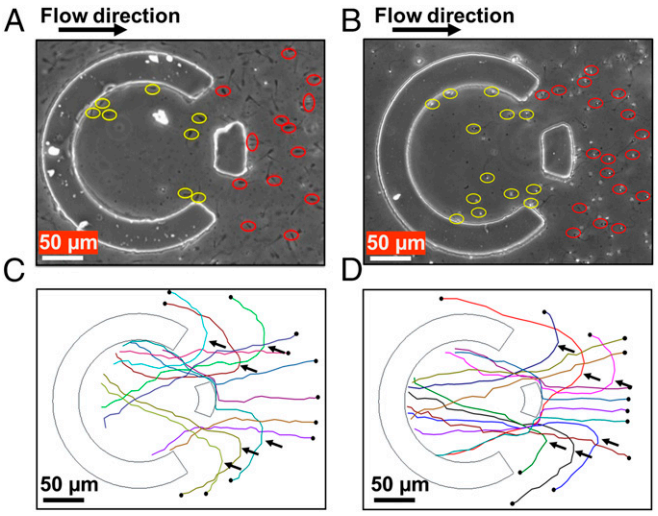

Fig. 3. Sperm undergoing rheotaxis in bovine and human samples. (*A*) Sperm with upstream swimming behavior before isolation in the bovine sample are detected and indicated with red ovals, whereas the isolated sperm are indicated with yellow ovals. (*B*) We similarly labeled sperm in the human sample with red and yellow ovals to indicate upstream-swimming and isolated sperm, respectively. (*C*) Trajectories of 20 different sperm in the bovine sample are depicted. All trajectories begin at the solid black circles (●). (*D*) Trajectories of human sperm nearby and inside the corral are also shown. In *C* and *D*, the trajectories that show a change in sperm orientation due to rheotaxis are indicated with arrows.

(~10–30 μL·min^{-1}) produces a moderate velocity field in front of the corral, the maximum abundance for the human sperm occurs for those displaying a velocity of 55–65 μm·s^{-1}. The corresponding velocity range of the most abundant captured bovine sperm was 70–80 μm·s^{-1}. Overall, we observe that most of the sperm in the collected samples are motile and normal in morphological appearance. The robust performance of this device at different injection flow rates suggests the rheotaxis-based separation is successful and consistent under different conditions. The velocity distribution of the isolated sperm remains nearly constant despite user variability and small variations in the fluid flow rate, which is a common and inevitable noise source in all injection systems.

Furthermore, as established in the velocity distributions of *SI Appendix*, Fig. S7, there is a lower cutoff for the velocity of the isolated sperm. This minimum cutoff is principally related to the injection rate and depends on the type (i.e., the species used) and quality of the semen sample. In *SI Appendix*, Fig. S7, we demonstrate that the number of sperm with motilities lower than the minimum cutoff (40 μm·s^{-1}) is zero. These zero values confirm that the entrance of dead sperm and sperm with low motilities is hampered; hence, this device ensures that all isolated sperm are normally motile. This level of isolation efficiency (up to 100%) is desirable for ARTs as an alternative to current sperm separation methods.

Tunable Isolation of Sperm Based on Motility. The last characteristic of our device is its motility-based tunability in sperm selection. As described previously, when the flow rate increases, sperm will be selected in a narrower motility range based upon rheotactic behavior and the ability of the sperm to overcome the fluid flow, causing the minimum sperm velocity cutoff to increase (*SI Appendix*, Fig. S7). When the injection rate increases, sperm with motilities lower than the new cutoff cannot swim upstream, and consequently cannot enter the corral, while sperm with high motility are still able. As such, we can use the injection rate to control the motility range of the separated sperm. In the data presented herein, we demonstrate that we can hinder sperm with motilities lower than 55 μm·s^{-1} in human samples and lower than 53 μm·s^{-1} in bovine samples from entering the corral. This similarity between the cutoff for human and bovine sperm may underlie a similarity between their locomotive structures and strategies.

Sperm Retainers and Residence Time in the Corral. Upon entrance to the corral, the sperm begin to move with their own propulsive force since the velocity field of the sperm medium is zero in this area. Once a sperm reaches the interior wall of the corral, because of its hydrodynamic interaction with the structure, it starts to move parallel to the wall, and consequently exits back into the microfluidic channel (Movies S1 and S2). The residence time of sperm inside this corral design is 10.2 ± 4.6 s and 12.3 ± 3.4 s for bovine and human sperm, respectively, and can be either increased or decreased by changing the size of the corral. As a result, this type of structure can be used for sperm entrapment for a limited time interval, which is still useful for many applications, such as investigating the response of sperm to drug exposure.

To retain all captured sperm inside the corral, which is imperative for sperm sample preparation and ART applications, we designed sperm retainers inside the corral (Fig. 4*A*). Sperm retainers enabled the corral to keep all trapped motile sperm inside, as the extracted trajectories in Fig. 4*B* confirm. Following the interior wall, the sperm eventually encounter the corners provided by the retainers, and therefore cannot follow the wall any further, as can be seen in Fig. 4 *C* and *D* and Movies S3 and S4 for both bovine and human sperm, respectively. If, by any chance, the sperm could escape the corner, the interior wall steer them again to the inside of the corral.

The sperm retainer design made the corral system extremely stable. All captured sperm (~150 sperm for a poor bovine sample and ~600 sperm for a normal human sample after a 2-min sample injection) remained within the corral even after washing the semen sample from the main channel with Tyrode's albumin lactate pyruvate (TALP) using a flow rate of 5 mL·h^{-1}, as can be seen in Movies S5 and S6. To retrieve the isolated sperm sample, we washed the chip at a higher flow rate of 5 mL·h^{-1} also using TALP. This amount of shear/flow rate, which is very low in comparison to human and bovine ejaculation, is also much smaller in comparison to the forces sperm experience in conventional separation methods.

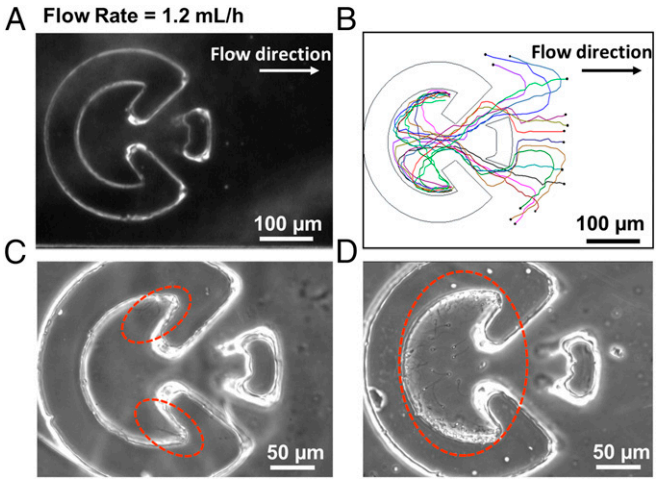

Fig. 4. Enhanced sperm retention using a modified corral structure. (*A*) Microfluidic corral device with sperm retainers. (*B*) Trajectories extracted for human sperm entering the corral. All of the sperm remained inside the corral by being captured in the corners or following the interior walls of the retainers. (*C*) Bovine semen sample was injected, and the motile sperm entered the corral and remained inside. (*D*) Human semen sample was injected, and the corral captured and maintained the motile sperm. The dashed red ovals indicate the motile sperm captured by the corral.

One hundred percent of the isolated sperm within the corrals are motile, demonstrating the incredible efficiency of the device as judged by the velocity distribution of the separated sperm sample. However, another measure of the device's efficiency is in terms of the total number of isolated sperm in each corral. We were able to isolate 1.94 ± 0.32% (1.56 ± 0.1%), 1.03 ± 0.11% (0.98 ± 0.08%), and 0.32 ± 0.07% (0.32 ± 0.04%) of the motile and viable human (bovine) sperm inside each corral at flow rates of 0.6 mL·h^{-1}, 1.2 mL·h^{-1}, and 1.8 mL·h^{-1}, respectively (*SI Appendix*, Figs. S8–S10). Although we demonstrate that the number of captured sperm is determined by the motile vs. nonmotile sperm ratio of the sample, the percentage of the motile sperm that are captured by each corral is solely determined by the injection rate.

Conclusion

The viability and motility of sperm in a semen sample are vital for mammalian reproduction. Several centrifugation-based methods are currently used to separate motile sperm from semen samples to increase the effectiveness of various ARTs. These conventional methods are time-consuming and labor-intensive, and they have been reported to be detrimental to the morphology and paternal content of the sperm. In this work, we have proposed a microfluidic high-throughput device that can passively separate motile sperm from the rest of the semen sample. The passive nature of our device promises to conserve the viability and quality of the sperm for applications such as in vitro fertilization.

The design of our microfluidic system for sperm separation relied upon the generation of rheotaxis zones in front of a microfluidic corral system. We experimentally measured the minimum shear rate within the rheotaxis zone for sperm to undergo rheotaxis. Additionally, by experimentally extracting the sperm movement distribution within the rheotaxis zone, we

demonstrated the role of rheotaxis in increasing the number of corralled sperm. Moreover, by providing a model for sperm movement inside the rheotaxis zone, and comparing that with experimental data, we can quantify the motility-based selection of our device as a function of flow/shear rate.

Our microfluidic device is simple to use and effective, corralling only sperm with progressive and normal motility capable of upstream swimming and ensuring that the number of dead sperm within the corral is zero, resulting in a separation efficiency of 100%. We have also demonstrated that sperm separation by our device is dependent on flow rate. By using different fluid injection rates (0.6 $mL{\cdot}h^{-1}$, 1.2 $mL{\cdot}h^{-1}$, and 1.8 $mL{\cdot}h^{-1}$), our device is capable of selecting sperm with motilities higher than a tunable minimum cutoff. Additionally, we demonstrated how retainers fabricated inside the corral system increased the residence time of the sperm within the corral from ~12 s to 45 min.

We believe these findings have a broad range of applications, including the dairy and beef industry, as we have demonstrated the device can be used to separate motile bovine sperm as well. Our device could further be used for clinical studies on human sperm and for ARTs.

Materials and Methods

Human and Bovine Sperm Medium. The human semen sample was generously provided by Weill Cornell Medicine in accordance with the Weill Cornell Medicine Institutional Review Board (IRB) guidelines. An approved IRB consent form was used to prospectively recruit patients interested in participating in this study. This fresh semen sample was first diluted with TALP medium (24) and kept at a constant temperature of 37 °C for the duration of the experiment. Commercially available cryopreserved bovine samples from four different bulls were generously donated by Genex Cooperative. Semen from two of the bulls was frozen in a milk-based extender, and semen from the other two bulls was frozen in an egg yolk-based extender in 250-μL straws at a concentration of 100 million sperm per milliliter. The frozen straws were thawed in a 37 °C water bath and diluted 1:1 with TALP medium before use. After dilution, the dynamic viscosity of the human and bovine sperm samples was 3.42 $mPa{\cdot}s^{-1}$ and 2.11 $mPa{\cdot}s^{-1}$, respectively. In the experiments, we used 10 replicates of the bovine samples and three replicates of the human sample.

Device Fabrication and Injection Systems. We used conventional soft lithography (36) to fabricate the microfluidic device out of polydimethylsiloxane. Syringe pumps (Chemyx Fusion 200) were used to control the flow rate of the sperm medium at different injection rates of 0.6 $mL{\cdot}h^{-1}$, 1.2 $mL{\cdot}h^{-1}$, and 1.8 $mL{\cdot}h^{-1}$.

Image and Video Acquisition. Images and video recordings were acquired at 25 frames per second using phase contrast microscopy with a 10× objective and a digital Neo CMOS camera. During the experiments, the microfluidic chip was kept on a heated 37 °C microscope stage (Carl Zeiss). The average path velocity of the sperm was determined using ImageJ (version 1.51j8; NIH) and MATLAB (Version R2017a; MathWorks) software by measuring the average distance between the center of the sperm head in each frame divided by the time elapsed.

Simulation Software. The layout of the microfluidic device was imported into COMSOL MULTIPHYSICS (version 5.2) simulation software. Using the laminar fluid module in stationary mode, we solved the Navier–Stokes (Eq. **2**) and conservation of mass (Eq. **3**) equations with a no-slip boundary condition at the walls. The simulations were performed for 11 input flow rates between 10 $\mu L{\cdot}min^{-1}$ and 30 $\mu L{\cdot}min^{-1}$ at steps of 2 $\mu L{\cdot}min^{-1}$:

$$\rho(\mathbf{v}.\nabla\mathbf{v}) = -\nabla p + \nabla.\mu\left(\nabla\mathbf{v} + (\nabla\mathbf{v})^{T}\right), \quad [2]$$

$$\nabla.\mathbf{v} = 0, \quad [3]$$

where v denotes the velocity field, ρ is the density of the sperm medium, p is pressure, and μ is the dynamic viscosity.

ACKNOWLEDGMENTS. We thank Dr. Gianpiero Palermo's lab for providing the human semen sample used in this study. We also thank Farhad Javi and Marry Godec for their assistance in illustrations and proofreading the paper. This work was performed, in part, at the Cornell NanoScale Facility, a member of National Nanotechnology Coordinated Infrastructure (NNCI), which is supported by National Science Foundation Grant ECCS-1542081.

1. Suarez SS, Pacey AA (2006) Sperm transport in the female reproductive tract. *Hum Reprod Update* 12:23–37.
2. Tulsiani D (2012) *Introduction to Mammalian Reproduction* (Springer, New York).
3. Guzick DS, et al.; National Cooperative Reproductive Medicine Network (2001) Sperm morphology, motility, and concentration in fertile and infertile men. *N Engl J Med* 345:1388–1393.
4. Alvarez JG, et al. (1993) Centrifugation of human spermatozoa induces sublethal damage; separation of human spermatozoa from seminal plasma by a dextran swim-up procedure without centrifugation extends their motile lifetime. *Hum Reprod* 8:1087–1092.
5. Yanagida K, et al. (1999) Successful fertilization and pregnancy following ICSI and electrical oocyte activation. *Hum Reprod* 14:1307–1311.
6. Parrish JJ, Krogenaes A, Susko-Parrish JL (1995) Effect of bovine sperm separation by either swim-up or Percoll method on success of in vitro fertilization and early embryonic development. *Theriogenology* 44:859–869.
7. Kimura Y, Yanagimachi R (1995) Intracytoplasmic sperm injection in the mouse. *Biol Reprod* 52:709–720.
8. Cho BS, et al. (2003) Passively driven integrated microfluidic system for separation of motile sperm. *Anal Chem* 75:1671–1675.
9. Aitken RJ, Clarkson JS (1988) Significance of reactive oxygen species and antioxidants in defining the efficacy of sperm preparation techniques. *J Androl* 9:367–376.
10. Friedrich BM, Jülicher F (2007) Chemotaxis of sperm cells. *Proc Natl Acad Sci USA* 104: 13256–13261.
11. Miki K, Clapham DE (2013) Rheotaxis guides mammalian sperm. *Curr Biol* 23:443–452.
12. Suarez SS, Ho H-C (2003) Hyperactivated motility in sperm. *Reprod Domest Anim* 38: 119–124.
13. Suarez SS (1996) Hyperactivated motility in sperm. *J Androl* 17:331–335.
14. Suarez SS (2016) Mammalian sperm interactions with the female reproductive tract. *Cell Tissue Res* 363:185–194.
15. Wassarman PM, Litscher ES (2001) Towards the molecular basis of sperm and egg interaction during mammalian fertilization. *Cells Tissues Organs* 168:36–45.
16. Eisenbach M, Giojalas LC (2006) Sperm guidance in mammals–An unpaved road to the egg. *Nat Rev Mol Cell Biol* 7:276–285.
17. Denissenko P, Kantsler V, Smith DJ, Kirkman-Brown J (2012) Human spermatozoa migration in microchannels reveals boundary-following navigation. *Proc Natl Acad Sci USA* 109:8007–8010.
18. Seo D, Agca Y, Feng ZC, Critser JK (2007) Development of sorting, aligning, and orienting motile sperm using microfluidic device operated by hydrostatic pressure. *Microfluid Nanofluid* 3:561–570.
19. Koh JBY, Marcos (2015) The study of spermatozoa and sorting in relation to human reproduction. *Microfluid Nanofluid* 18:755–774.
20. Li G, Tang JX (2009) Accumulation of microswimmers near a surface mediated by collision and rotational Brownian motion. *Phys Rev Lett* 103:078101.
21. Tung CK, et al. (2015) Emergence of upstream swimming via a hydrodynamic transition. *Phys Rev Lett* 114:108102.
22. Zöttl A, Stark H (2012) Nonlinear dynamics of a microswimmer in Poiseuille flow. *Phys Rev Lett* 108:218104.
23. Nosrati R, Driouchi A, Yip CM, Sinton D (2015) Two-dimensional slither swimming of sperm within a micrometre of a surface. *Nat Commun* 6:8703.
24. Tung CK, et al. (2015) Microgrooves and fluid flows provide preferential passageways for sperm over pathogen Tritrichomonas foetus. *Proc Natl Acad Sci USA* 112:5431–5436.
25. Bukatin A, Kukhtevich I, Stoop N, Dunkel J, Kantsler V (2015) Bimodal rheotactic behavior reflects flagellar beat asymmetry in human sperm cells. *Proc Natl Acad Sci USA* 112:15904–15909.
26. Elgeti J, Winkler RG, Gompper G (2015) Physics of microswimmers–Single particle motion and collective behavior: A review. *Rep Prog Phys* 78:056601.
27. Smith GD, Takayama S (2017) Application of microfluidic technologies to human assisted reproduction. *Mol Hum Reprod* 23:257–268.
28. Tasoglu S, et al. (2013) Exhaustion of racing sperm in nature-mimicking microfluidic channels during sorting. *Small* 9:3374–3384.
29. Nosrati R, et al. (2017) Microfluidics for sperm analysis and selection. *Nat Rev Urol* 14: 707–730.
30. Schuster TG, Cho B, Keller LM, Takayama S, Smith GD (2003) Isolation of motile spermatozoa from semen samples using microfluidics. *Reprod Biomed Online* 7: 75–81.
31. Modak N, Datta A, Ganguly R (2009) Cell separation in a microfluidic channel using magnetic microspheres. *Microfluid Nanofluid* 6:647–660.
32. Devenica LM, Grimm B, Hultum T-A, Carter AR (2017) Progress on an optical trapping assay to measure DNA folding pathways in sperm. *Proc SPIE Int Soc Opt Eng*, 10.1117/12.2275722.
33. Zhang Z, et al. (2016) Human sperm rheotaxis: A passive physical process. *Sci Rep* 6: 23553.
34. Kantsler V, Dunkel J, Blayney M, Goldstein RE (2014) Rheotaxis facilitates upstream navigation of mammalian sperm cells. *eLife* 3:e02403.
35. Tung CK, Ardon F, Fiore AG, Suarez SS, Wu M (2014) Cooperative roles of biological flow and surface topography in guiding sperm migration revealed by a microfluidic model. *Lab Chip* 14:1348–1356.
36. Xia Y, Whitesides GM (1998) Soft lithography. *Angew Chem Int Ed Engl* 37:550–575.